Continuous Wavelet Analysis for Spectroscopic Determination of Subsurface Moisture and Water-Table Height in Northern Peatland Ecosystems

Asim Banskota, Michael J. Falkowski, Alistair M. S. Smith, Evan S. Kane, Karl M. Meingast, Laura L. Bourgeau-Chavez, Mary Ellen Miller, and Nancy H. French

***Abstract*— Climate change is altering the water-table (WT) height and near-surface moisture conditions in northern peatlands, which in turn both increases the susceptibility to fire and reduces the carbon sink capacity of these ecosystems. To further develop remote sensing-based measurements of peatland moisture characteristics, we employed coincident surface reflectance and moisture measurements in two Sphagnum moss-dominated peatland sites. We applied the Mexican hat continuous wavelet transform to the measured spectra to generate wavelet features and coefficients across a range of scales. Overall, wavelet analysis was an improvement over the previously tested spectral indices at both the study sites. Linear mixed effect models for WT height using wavelet features accounted for more of the variance with both an improved marginal R^2 (29% greater) and a larger conditional R^2 (21% greater) compared to the best performing spectral index. While spectral indices performed similarly with wavelet coefficients for moisture content measured at 3 cm depth, they performed poorly for volumetric moisture content measured at 7 cm depth. The current study also revealed the advantage of selecting the best subsets of wavelet features based upon genetic algorithm over a more widely used technique that selects features based on correlation scalograms. It also provided new insights into the significance of various spectral regions to detect WT alteration-induced vegetation change.**

***Index Terms*— Genetic algorithm (GA), hyperspectral, peat moisture, vegetation indices, wavelet transform.**

Manuscript received March 18, 2015; revised May 15, 2016 and August 26, 2016; accepted September 30, 2016. Date of publication December 21, 2016; date of current version February 23, 2017. This work was supported in part by the NASA Terrestrial Ecology Program under Grant NNX14AF96G, Grant NNX12AK31G, and Grant NNX09AM156, in part by the Joint Fire Sciences Program under Grant L11AC20267-JFSP 11-1-5-16, in part by The National Science Foundation under Grant DEB-1146149, in part by the U.S. Department of Agriculture Forest Service, and in part by the MTU Ecosystem Science Center. *(Corresponding author: Asim Banskota.)*

A. Banskota is with Monsanto, St. Louis, MO 63146 USA (e-mail: asimbanskota@gmail.com).

M. J. Falkowski is with the Department of Ecosystem Science and Sustainability, Colorado State University, Fort Collins, CO 80523 USA.

A. M. S. Smith is with the Department of Forest, Rangeland, and Fire Sciences, University of Idaho, Moscow, ID 83844 USA.

E. S. Kane and K. M. Meingast are with the School of Forest Resources and Environmental Science, Michigan Technological University, Houghton, MI 49931 USA.

L. L. Bourgeau-Chavez, M. E. Miller, and N. H. French are with Michigan Tech Research Institute, Michigan Technological University, Ann Arbor, MI 49931 USA.

Color versions of one or more of the figures in this paper are available online at http://ieeexplore.ieee.org.

Digital Object Identifier 10.1109/TGRS.2016.2626460

I. Introduction

PEATLAND ecosystems, which are distributed mainly across boreal and subarctic regions, likely reserve >30% of soil organic carbon (470–620 Pg), despite representing only about 3% of the global land surface [1], [2]. The accumulation of peatland carbon generally depends on flooded conditions that impede rates of decomposition. Thus, the formation and maintenance of boreal peatlands are influenced by site conditions that maintain a high water-table (WT) (such as the presence of perennially frozen ground and changes in precipitation patterns and hydrology [3]). The strong controls of climate and hydrology on peat formation make peatlands particularly sensitive to climatic conditions [4], [5]. As such, monitoring tools for measuring WT position and near-surface moisture contents in a changing climate are needed to understand the potential changes in peatland carbon balance, and would greatly inform modeling efforts to understand the peatland carbon dynamics. (see [6], [7]).

Collecting detailed ground-based hydrological measurements in peatlands over large spatial scales is extremely challenging. However, *Sphagnum* mosses, which often dominate ground cover in northern peatlands, are highly sensitive to changes in the near-surface moisture condition and WT position [8]. Due to *Sphagnum* mosses' physiology, their hydrological conditions can often be inferred via changes in their surface reflectance [8]–[12]. Remote sensing has been widely used to infer the moisture content of vegetation and fuels [13]–[15]. Assessments of surface moisture content and WT position typically employ spectral indices leveraging the near infrared (NIR) and short wave infrared (SWIR) regions of the electromagnetic spectrum. Usually, one of the bands related to strong water absorption regions are used in combination with an NIR band as a reference to normalize the effect of background and vegetation structure variability. For example, Harris *et al*. [10] and Meingast *et al*. [12] employed the floating water band index (fWBI) in the NIR and moisture stress index (MSI) in the SWIR to assess the *Sphagnum* moisture status and WT position in peatland ecosystems. They reported high correlations between the *Sphagnum* surface moisture content and both fWBI and MSI. Highly significant

0196-2892 © 2016 IEEE. Personal use is permitted, but republication/redistribution requires IEEE permission.
See http://www.ieee.org/publications_standards/publications/rights/index.html for more information.

relationships were also reported between these spectral indices and the WT position [11], [12].

Although many studies (see [9]–[11], [16]) have employed remote sensing data to characterize the peatland moisture status and WT positions, relationships have typically been assessed based on individual *Sphagnum* plants and relatively homogeneous *Sphagnum* canopies. These studies were also often constrained by field measurements being confined to ranges typical of nondrought conditions or seasonally high WT positions. Building on these studies, Meingast *et al.* [12] tested the utility of a suite of spectral indices for assessing moisture conditions through a series of manipulation experiments in both small experimental plots (mesocosms) and extended field studies representing a broad range of WT positions as well as mixed species assemblages. They found a strong relationship between spectral indices and near-surface moisture condition (3 cm depth) in the field, but the relationship weakened for WT height and moisture content at greater depths (7 cm) at the experimental plots. The moisture variation was greater at the experimental plots as experimental manipulations ranged from extreme drought to high WT conditions. Studies carried out in forested ecosystems have demonstrated that models employing spectral indices perform poorly in areas that have large variation in moisture values [17], [18]. The vegetation spectral response to changes in moisture content vary across the NIR and SWIR regions: as moisture content decreases, the strong water absorption features become weaker, the amplitude of SWIR region increases, and the absorption features corresponding with leaf dry matter constituents (e.g., protein, lignin and cellulose) become more apparent [18]. As such, spectral indices that only employ 1–2 water absorption features often do not capture the full range of moisture variations-induced spectral changes.

Wavelet analysis has recently emerged as a promising remote sensing analysis tool for analyzing spectral variations that occur at multiple discrete wavelengths or for analyzing spatial assemblages of similar spectral values that exist over a range of discrete sizes [19], [29]. Vegetation reflectance is governed by a suite of parameters, including leaf pigments, moisture content, leaf dry matter, vegetation structure, and background reflectance, among others. The sensitivity of reflectance to these parameters is scale dependent, as some impact reflectance locally across a narrow range (e.g., chlorophyll) while other reflectance is evident over a broader region of the spectrum (e.g., vegetation structure). Furthermore, parameters such as leaf moisture content and dry matter impact reflectance across multiple scales (i.e., across narrow and broad absorption features) [23], [30]. Wavelet analysis, which transforms the reflectance spectrum into coefficients resolving at high scales (e.g., narrow absorption features) and low scales (e.g., broad absorption features), is well suited for analysis of signals that vary across multiple scales and wavelength positions. As such, wavelet analysis has been increasingly used in vegetation analysis via spectroscopic remote sensing. Recent studies have also demonstrated the utility of wavelet analysis for estimating leaf and canopy water estimation using field-based and imaging spectroscopy [18], [31]–[33].

The major step in wavelet analysis is the selection of an optimum number of wavelet coefficients associated with a given type of spectral feature [34]. This enables the identification of the range of characteristic scales the feature exists over that can be used to build an empirical model predicting an attribute of interest (e.g., moisture content). Cheng *et al.* [18] introduced a coefficients selection technique that is based upon the correlation between wavelet coefficients and moisture content. While this approach showed promise, it does not necessarily generate the optimal combination of wavelet coefficients that best describe the variation in the independent variable (e.g., moisture content). This is because a multiple regression model does not require that all dependent variables be highly correlated with the independent variable, rather they, in combination, provide the lowest modeling or prediction error. A potential alternative approach is to conduct wavelet coefficients selection using the theory of genetic algorithms (GAs), which is widely implemented by studies involving imaging spectroscopy for vegetation analysis [35]–[37]. Recently, it has also been explored and demonstrated as a useful technique for selecting wavelet coefficients [28], [38], [39].

As a result, the overarching goal of this study is to evaluate the utility of spectroscopic wavelet analysis to improve understanding of moisture dynamics in peatland ecosystems. This is achieved via the analysis of data at an experimental peatland manipulation facility as well as at a natural peatland site. Specifically, we seek to answer three questions as follows.

1) Is spectroscopic wavelet analysis an effective means to characterize peatland moisture dynamics?
2) What is the most efficient means for selecting the wavelet coefficients in that analysis of spectroscopy data?
3) What spectral regions (of multiple scales) are influenced by moisture variation?

To answer the first question, we compare wavelet-derived moisture estimates with moisture estimates derived via spectral indices used in previous studies to estimate the moisture of peatland vegetation. The second question is addressed via a comparison of two coefficient selection strategies, a GA approach and an approach based on correlation scalogram. We analyzed different wavelet coefficients with respect to their scales and wavelength positions to answer the third question.

II. Methods

A. Study Sites

This study utilized the data set collected and described in [12]. The data set was collected at two sites, one outdoor peatland manipulation experimental facility and one natural peatland field site. The outdoor experimental facility allowed us to undertake spectral analysis under an extreme range of peatland moisture conditions and WT positions. The natural peatland field site facilitated additional assessment of the methods under conditions with greater heterogeneity in microtopography and vegetation structure. The sites and data collection methods are described in detail in [12].

The outdoor experimental facility, called PEATcosm (Peatland Experiment at The Houghton Mesocosm Facility) is located at the USDA Forest Service Northern Research Station

in Houghton, Michigan USA. The facility has 24 mesocosm bins containing intact monoliths of peat extracted from an extensive oligotrophic peatland in Meadowlands, MN (N47.07278°, W92.73167°) in May 2010. The peatland vegetation was dominated by the sedge *Carex oligosperma Michx.*, ericaceous shrubs *Chamaedaphne calyculata (L.) Moench., Kalmia polifolia Wangenh., Vaccinium oxycoccus L.* and the mosses *Sphagnum rubellum Wilson, Sphagnum magellanicum Brid., and Sphagnum fuscum (Schimp.) Klinggr*. Three vegetation treatments were created by manipulating the plant communities as described in detail in [40]: all ericaceous shrubs were removed in the sedge treatment, all sedges were removed in the ericaceae treatment, and the shrub and sedge communities were left intact in the unmanipulated treatment. The different water treatments in the PEATcosms were based on the long-term WT trends from the USDA Forest Service Marcell Experimental Forest (near the peat harvest sites).

The field site is located near Nestoria, MI (46°34′22.66″ N, 088°16′44.85″ W) and represents an extensive poor fen with a maximum peat depth exceeding 5 m and approximately 30 ha in size. Unlike the PEATcosm experiment, this field site allowed for destructive sampling for near-surface moisture determination. The vegetation community composition of this site was similar to that of PEATcosm. The overstory consists of *Larix laricina* and *Picea mariana* and the understory consists of mixed sedge (*Carex spp.*) and ericoid shrubs (*K. polifolia, C. calyculata, R. groenlandicum, A. polifolia var. glaucophylla, Vaccinium spp.*) with a *Sphagnum* moss ground cover. Three species of *Sphagnum* are present: *Spp. magellanicum, Spp. angustifolium, and Spp. fuscum*.

B. Reflectance Measurements

As described in [12], spectral data were collected using an ASD Fieldspec 3 spectroradiometer (Analytical Spectral Devices, Boulder, CO). The spectral measurements were conducted at both the PEATcosm facility and the Nestoria field site under clear and low haze conditions between 11:00 and 15:00 EDT. This spectroradiometer measures surface reflectance over the spectral range of 350–2500 nm, with a spectral resolution of 3 nm between 350 and 1000 nm (1.4 nm spectral interval) and 10 nm for wavelengths from 1000 and 2500 nm (2 nm spectral interval). A linear interpolation routine produced reflectance measurements at every 1 nm interval within the wavelength range of the instrument.

ASD measurements were conducted immediately prior to moisture and WT measurements at the PEATcosm facility. An average of five ASD samples was recorded within each bin from approximately 1 m above the vegetation surface using a steel sampling frame to attach the spectroradiometer. In the field study, systematic ASD measurements were taken at 10 m intervals along three transects across a gradient of moisture, canopy, and microtopographic conditions present at the site. In an effort to accurately characterize the heterogeneity in the system as well as increase the moisture variability in the data set, measurement locations were alternated between hummocks, lawns, and hollows. The spectral signatures from both the PEATcosm experiment and field study were processed using the statistical software package R (v3.0.1).

C. Moisture Measurements

Near-surface moisture [integrated 7 cm volumetric moisture content (VMC)] was measured in the PEATcosm based upon the apparent dielectric constant of the peat using a Thetaprobe (Delta-T Devices, Cambridge, U.K.). Output voltage signal was converted into VMC by applying a calibration equation based on peat samples from the Nestoria field site ($R^2 = 0.77$, RMSE – 0.13, $n = 20$). At the field site, cylinders of the *Sphagnum* peat material were harvested by passing a sharpened circular tin ring of 7 cm diameter through the peat canopy to a depth of 3 cm. The samples were separated across the bottom of the ring using a serrated knife. The fresh samples were inserted into a preweighed plastic bag and weighed. Upon returning from the field they were oven dried at 65 °C in a preweighed paper bag to determine the moisture weight of the samples. VMC was then calculated by multiplying moisture weight by bulk density. Thetaprobe moisture measurements were taken immediately following spectral measurements and immediately prior to vegetation harvesting at the field site to determine 7 cm VMC in a nondestructive manner.

D. Wavelet Analysis

Wavelet analysis resolves a signal over a range of scales by convolving the signal with a series of wavelet daughter functions $\{\psi\alpha,\ b(\lambda)\}$, which are generated by changing the dilation (i.e., scale parameter) and positions of the mother wavelet function ($\psi(\lambda)$ as (see [19], [25], [26], [34])

$$\varphi_{a,b}(\gamma) = \frac{1}{\sqrt{a}}\varphi\left(\frac{\gamma - b}{a}\right) \tag{1}$$

where $a > 0$ and represents the scaling factor defining the width of the wavelet and b is the translation parameter that determines the location in the signal. Representing the data at multiple scales by wavelet decomposition is somewhat analogous to looking at data with moving windows of different widths. The "gross" features (or trend) of the original data are resolved at larger scales and "fine" features or (high frequency variation) are resolved at small scales [22]. The final product of wavelet decomposition constitutes a set of wavelet coefficients that are a function of the scale of the analyzing wavelets and the position of the signal (part of the signal being analyzed).

Wavelet transforms are applied in two primary forms: discrete and continuous. In discrete analysis, wavelet coefficients are usually sampled at some discrete scale and positions, whereas in continuous wavelet transform (CWT), data are analyzed at all the possible scales and positions. In this paper, we chose the CWT because the scale component is directly comparable to the input reflectance spectrum on a band-by-band basis, and the results are easy to interpret [18]. The second derivative of a Gaussian function also known as the Mexican Hat wavelet was used as a mother wavelet basis since previous research has found it ideal for vegetation moisture estimation due to the similarity between the shape of absorption features and the shape of a Gaussian function. Since the wavelet decomposition across a continuum of possible scales would be computationally expensive and would ultimately lead to

large data volumes, a discrete approximation of the CWT was performed at dyadic scales $2^1, 2^2, 2^3, \ldots$, and 2^{10} [25]. CWT analysis of a single plot spectrum (2151 bands) in this case produces wavelet power scalogram of 2151×10 dimensions. Each element of the scalogram is the wavelet power, which refers to the magnitude of each wavelet coefficient that characterizes the correlation between a subset of the input spectrum and a scaled, shifted version of the mother wavelet [24]. For a simple representation of the scalograms, these scales are labeled as scales $1, 2, 3, \ldots$, and 10 in the following section and are comparable to the scales described in [18] and [23].

E. Wavelet Feature Selection Based Upon Correlation Scalograms

A commonly employed wavelet feature selection technique (see [18], [31], [32]) was used to identify the most important CWT coefficients for WT height and VMC. The method to select meaningful wavelet coefficients is comprised of four steps, which are described in detail in [18]. In Step 1, the CWT was applied to all reflectance spectra to calculate the wavelet power as a function of wavelength and scale. A correlation scalogram was then constructed in Step 2 by establishing R^2 between each element of the wavelet power scalograms and either WT or VMC. In Step 3, wavelet coefficients where the R^2 is not statistically significant ($p \geq 0.05$) are masked and the top 1% wavelet coefficients (as ranked by R^2) are extracted. In Step 4, wavelet coefficients with the maximum R^2 within each region are determined to represent the spectral information captured by the feature region. Eventually, a small number of sparsely distributed coefficients are selected representing these regions and capturing the most important information related to changes in either WT or VMC.

F. Wavelet Feature Selection Based Upon the Genetic Algorithm

The GA [41], which is widely used for solving a range of optimization problems, is a popular technique for variable selection. To determine the "fitness" of random subsets of variables, the GA takes cues from Darwin's biological theory of "natural selection" and "survival of the fittest" in which more genetically fit individuals have a greater chance of selection [42]. An initial run of the GA is set up with input parameters and a randomized population of variable subsets. A specified merit function (e.g., RMSE) assesses the fitness of each subset, with subsets below the average fit discarded. Subsets with greater fitness are allowed to survive and undergo exchange of variables (cross-breeding) and poor subsets are discarded. The iterative process converges once a predefined criterion is met, returning the best subset of variables.

In this paper, the GA was employed using the GA toolbox in MATLAB (version 7.1; Mathworks, Inc.). The algorithm was run separately for VMC and WT to build a range of models with different numbers of wavelet coefficients ($n = 2, 3, \ldots, 5$). Models with $n > 5$ were not searched for the purpose of parsimony. We used a leave-one-out cross-validation (CV-RMSE) between observed and predicted WT or VMC as the fitness function. To avoid multicollinearity, subsets with highly correlated variables (i.e., Pearson correlation coefficient greater than 0.8) were discarded. The GA was run five times for each data set to find the best subset of coefficients, with the following GA parameters found best in [26] for a similar purpose: 1) population = 100; 2) mutation rate = 0.5; 3) cross over rate = 0.7; and 4) stopping criterion = 500 generations or 25 generations with no improvement in the best fitness value.

TABLE I

SPECTRAL INDICES USED FOR VEGETATION MOISTURE CONTENT AND WT HEIGHT

Spectral Index	Acronym	Formula	Reference
Water Index	WI	R900/R970	[43]
Floating Water Band Index	$FWBI_{980}$	$R_{920}/\min(R_{960-1000})$	[43]

G. Spectral Indices

In order to assess the performance, WT-based peatland moisture estimates were benchmarked against two commonly used moisture-based spectral indices that were recently found to perform best for spectral assessment of VMC and WT [12]. Table I displays the equations used to calculate the spectral indices. The water index (WI) is a ratio-based spectral index that divides a reference wavelength (R900) where water does not strongly absorb electromagnetic radiation by a wavelength where water strongly absorbs electromagnetic radiation (R970). The fWBI is formulated so that the strong water absorption denominator is dynamic (i.e., it is automatically set as the minimum reflectance values across a water absorption band in the wavelength range 960–1000 nm). This dynamism can strengthen the index's response to vegetation moisture as water absorption features can shift significantly under varying degrees of plant water stress [43].

H. Statistical Analysis

For the PEATcosms study, spectral features were statistically related to VMC and WT positions using linear mixed effects models via the linear and nonlinear mixed effects models R package [44]. Spectral features represented three different subsets of independent variables: commonly used spectral indices (WI and FWBI980), CWT coefficients selected via the GA approach (CWT-GA), and CWT coefficients selected by the correlation scalogram approach (CWT-CS). Linear mixed effects models were used to account for repeated measurements on the same experimental unit at the PEATcosm facility (i.e., an individual PEATcosm bin). This was achieved by setting a random intercept for each experimental unit within the model. The mixed linear model was compared to a linear least squares regression model using a likelihood ratio test to further support the need for using mixed effects models to account for artifacts of repeated sampling over the same experimental units. Stepwise regression techniques were used to reduce the number of CWT-CS coefficients based on the overall model significance ($p = 0.05$). Model fits for mixed effects models were evaluated using the Akaike Information

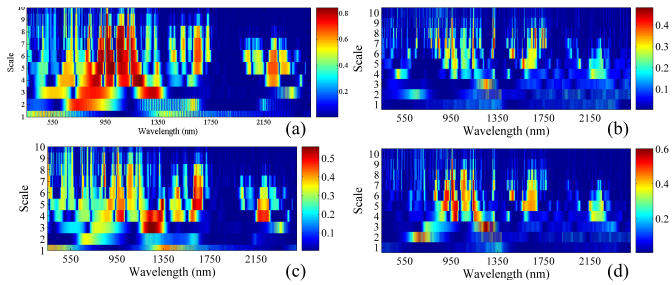

Fig. 1. Correlation scalograms for VMC and WT height (WT). (a) VMC 3 cm (Nestoria). (b) VMC 7 cm (Peatcosm). (c) VMC 7 cm (Nestoria). (d) WT (PEATcosm).

Criterion (AIC) as well as marginal R^2 [which describes the variance explained by fixed effects (i.e., spectral features)] and conditional R^2 [which describes the variance explained by the full model containing both fixed effects (i.e., spectral features) and random effects (i.e., experimental effects)] [45]. This was accomplished using the rsquared.glmm function in R (V3.0.1) [46].

For the field study, in which repeated measurements were not utilized, spectral indices were related to VMC and WT using least square regression. Simple linear regression was used to model the relationship of individual spectral indices (independent variable) with WT and VMC (dependent variable), while stepwise multiple regression was used to model the relationship between CWT features and WT and VMC. Models with variable n were subject to the following constraints: 1) all independent variables were significant at $a = 0.05$ and 2) there could not be multicollinearity, i.e., all variance inflation factors (VIFs) had to be less than 10. The regression residuals for all the selected models were tested for normality using the Lilliefors test [47]. A leave-one-out CV was then used to evaluate and rank competing models.

III. Results

Correlation scalograms for VMC and WT at the two study sites are shown in Fig. 1, which displays R^2 between the dependent variable (either WT or VMC) and CWT coefficients related to a specific wavelength and scale (1–10). Although the magnitude of the correlations is different, a similar pattern is exhibited in all the plots (i.e., the strongest correlation occurs in the wavelength range of 600–1350 nm at different scales and moderate correlations occur in the SWIR region of 1650 and 2200 nm at different scales).

The strongest relationship was observed between CWT coefficients and 3 cm VMC at the Nestoria field site, while somewhat weaker relationships were observed at the PEATcosm site. Based on each correlation scalogram and the four steps described in Section II-E, 10–12 CWT coefficients were extracted. Table II shows the number of coefficients extracted, as well as their wavelength positions and wavelet scales. The selected coefficients ranged from visible to SWIR depending upon the sites and variables of interest, and primarily represented three weak water absorption regions (950–970, 1150–1260, and 1520–1540 nm). The selected CWT coefficients comprised of both low (minimum 2) and high scale (maximum 9) coefficients.

TABLE II

CWT Coefficients and Their Related Wavelet Scales Selected Based Upon the Correlation Scalogram Analysis. The Final Subset of Selected Coefficients and Their Corresponding Scales Derived via Stepwise Regression Are Highlighted in Bold

Sites	Dependent variable	CWT coefficients selected by correlation scalogram	
		Wavelength (in nm)	Scale
PEATcosm	WT	**680**, 809, 825, 919, **955**, 1061, 1141, 1231, 1482, 1653, **2148**	**2**, 6, 6, 6, **7**, 7, 7, 3, 6, 5, **5**
	VMC (7 cm)	**653**, 777, **840**, 905, **955**, 1139, 1241, 1318, 1481, **1740**	**8**, 7, **7**, 9, **7**, 7, 3, 7, 6 **8**
Nestoria	VMC (3 cm)	733, 810, 823, 901, 939, **968**, 1057, **1246**, 1655, 2228	2, 7, 9, 5, **7**, 6, **7**, 4, 7, 5
	VMC (7 cm)	891, 929, **968**, 1070, 1246, **1340**, 1475, 1615, 1667, 2180	5, 9, 4, 9, 3, **5**, 6, 5, 5, 4

TABLE III

Model Statistics for the Best Models With Different Numbers of CWT Coefficients (2–5) Selected by the GA; CV-RMSE and CV-R^2 Refer to RMSE and R^2 From a Leave-One-Out CV, Respectively

Sites	Variable	n	RMSE	CV-RMSE	R^2	CV-R^2	Adjusted R^2
PeatCOSM	WT	2	5.8	5.9	0.75	0.73	0.74
		3	5.6	5.8	0.76	0.74	0.75
		4	4.8	4.8	0.83	0.81	0.82
		5	4.6	4.6	0.86	0.84	0.85
	7 cm VMC	2	0.08	0.08	0.66	0.63	0.65
		3	0.08	0.08	0.69	0.67	0.68
		4	0.07	0.07	0.74	0.70	0.72
		5	0.07	0.07	0.77	0.72	0.75
Nestoria	3 cm VMC	2	0.01	0.01	0.87	0.86	0.86
		3	0.01	0.01	0.88	0.86	0.87
		4	0.01	0.01	0.89	0.85	0.87
		5	0.01	0.01	0.89	0.85	0.87
	7 cm VMC	2	0.11	0.12	0.65	0.63	0.64
		3	0.10	0.11	0.71	0.67	0.70
		4	0.10	0.10	0.75	0.72	0.74
		5	0.09	0.09	0.76	0.73	0.65

Stepwise regression models combining a number of coefficients were then investigated for estimating VMC and WT. A stepwise regression model based upon model significance ($p = 0.05$) selected three CWT coefficients [centered on 680 nm (scale 2), 955 nm (scale 7), and 2158 nm (scale 5)] for WT and three for CWT coefficients [653 nm (scale 8), 840 nm (scale 7), 955 nm (scale 47), and 1740 nm (scale 8)] at the PEATcosm site. At Nestoria site, two CWT coefficients were selected for both 3 cm VMC [968 nm (scale 7) and 1246 nm (scale 47)] and 7 cm VMC [968 nm (scale 4) and 1340 nm (scale 5)]. The CWT coefficients selected by stepwise regression for VMC and WT are highlighted in bold in Table II.

A. Wavelet Coefficients and Spectral Bands Selected by GA

The GA was run to select models with $n = 2$–5 wavelet coefficients. The results of model selection using GA for either VMC or WT are presented in Table III. The table shows the number of wavelet coefficients selected, their central

TABLE IV

CENTER WAVELENGTH OF SELECTED CWT COEFFICIENTS BY GA AND RELATED WAVELET SCALE IN TWO STUDY SITES

Sites	Dependent variable	CWT coefficients selected by GA Wavelength (in nm)	Scale
PEATcosm	WT (in cm below peat surface)	720, 1148, 1549, 1735, 1242	4, 7, 10, 6, 3
	VMC 7 cm (cm^3 cm^{-3})	535, 711, 741, 959, 2364,	4, 5, 10, 7, 8
Nestoria	VMC 3 cm (cm^3 cm^{-3})	1066, 1258,1559	5, 4, 6
	VMC 7 cm (cm^3 cm^{-3})	595, 1158, 1550, 1592	6, 9, 8, 5

TABLE V

SUMMARY STATISTICS OF REGRESSION MODELS FOR SURFACE VMC TO WAVELET COEFFICIENTS AND SPECTRAL INDICES IN THE NESTORIA

Water table position	Variables	R^2	CV-R^2	RMSE	CV-RMSE	Adj-R^2
3 cm VMC	WI	0.83	0.82	0.02	0.02	0.83
	$fBWI_{980}$	0.86	0.85	0.02	0.02	0.86
	CWT-GA	0.88	0.86	0.01	0.01	0.87
	CW-CS	0.86	0.84	0.02	0.02	0.85
7cm VMC	WI	0.52	0.50	0.13	0.13	0.51
	$fBWI_{980}$	0.53	0.51	0.13	0.13	0.52
	CWT-GA	0.76	0.73	0.09	0.09	0.65
	CW-CS	0.60	0.56	0.12	0.12	0.59

wavelength position and wavelet scale, as well as model fit and CV statistics. CV-RMSE and CV-R^2 refer to RMSE and R^2 calculated based upon the leave-one-out CV, respectively. The results demonstrate that both calibration and CV accuracy improved with an increasing number of CWT coefficients for WT. For example, CV-R^2 and CV-RMSE improved from 0.73 to 0.84 and 5.9 to 4.8 cm for VMC and WT, respectively, for models with five wavelet coefficients compared to models with only two wavelet coefficients. The number of selected coefficients for each data set and their respective scales in relation to absorption features are provided in Table IV. Similar to the WT results, the best subset selected by GA comprised of five coefficients for 7 cm VMC at the PEATcosm site. At the Nestoria site, little improvement in CV accuracy was achieved after adding additional wavelet coefficients beyond two for 3 cm VMC and four for 7 cm VMC. Hence, the respective number of coefficients was chosen for each variable for final model building. As with coefficients selected by the correlation scalogram approach, wavelet coefficients were selected from a range of wavelet scales and mainly represented three weak water absorption regions (950–970, 1150–1260, and 1520–1540 nm) except for 7 cm VMC at PEATcosm where only one feature related to a water absorption region (959 nm) was selected.

B. Regression Results at the Nestoria Site

The results of the final models for VMC in Nestoria are shown in Table V. The first column in the table shows the dependent variable used in the regression model. CWT-GA and CWT-CS refer to the wavelet coefficients

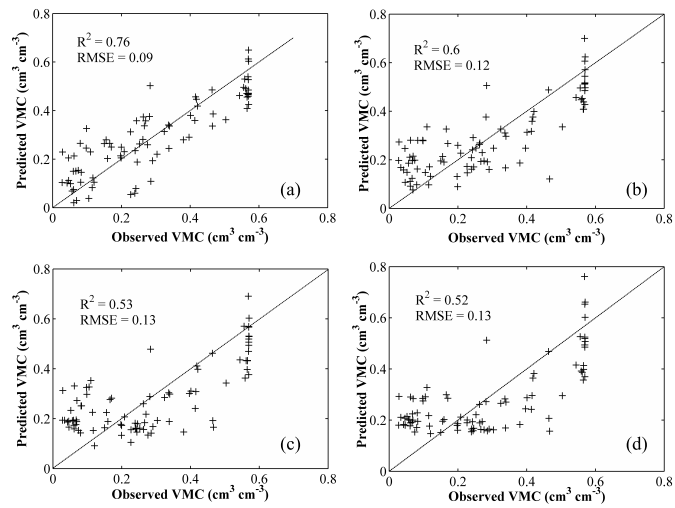

Fig. 2. Predicted versus observed plots related to surface 7 cm VMC (cm^3 cm^{-3}) at the Nestoria field site using spectral indices and wavelet features. Independent variables are (a) wavelet feature selected from GA, (b) wavelet features selected from the correlation scalogram, (c) fBWI980, and (d) WI.

selected by the GA analysis and by the correlation scalogram analysis, respectively. The linear regression results for both 3 and 7 cm VMC demonstrate that the model derived from CWT-GA provided the best fit (as indicated by greatest R^2 and lowest RMSE) as well as the best prediction accuracy (as indicated by CV R^2 and RMSE). All 3 cm VMC models were associated with a high statistical fit (CV R^2) and low RMSEs with slight differences among models. In contrast, greater differences in the model statistics occurred between the models based upon CWT-GA (CV-R^2 = 0.76, CV-RMSE = 0.09) and spectral indices [WI (CV-R^2 = 0.50, CV-RMSE = 0.13) and fBWI980 (CV-R^2 = 0.51, CV-RMSE = 0.13)] for 7 cm VMC. Models based upon CWT-GA performed better compared with models based upon CWT-CS (CV-R^2 = 0.56, CV-RMSE = 0.12). The independent tests for all the regression residuals did not reject the null hypothesis that the residuals come from a normal distribution ($p = 0.05$). VIF for all the variables was less than 10 in wavelet-based models, which implies absence or little multicollinearity among variables in the multiple regression model. Further analysis demonstrated strong relationships between observations and predictions with minimal bias for models based upon CWT-GA [Fig. 2(a)]. In contrast, the relationship between observations and predictions were poor for spectral indices with only a few data points lying close to the 1:1 line [Fig. 2(c) and (d)].

C. Mixed-Effects Regression Results at the PEATcosm Site

According to the linear mixed effects models, CWT coefficients were more strongly related to WT compared with the spectral indices assessed (Table VI). The strongest relationship to WT position was observed for the model built with CWT-GA followed by CWT-CS, with marginal R^2 values of 0.85 and 0.68, respectively. The mixed effect models for CWT coefficients produced smaller AIC and Bayesian Infor-

TABLE VI
MODEL STATISTICS FOR MIXED EFFECTS MODELS COMPARING WAVELET COEFFICIENTS AND SPECTRAL INDICES. CONTINUOUS WAVELET COEFFICIENTS INCLUDE THOSE SELECTED BY THE GA (CWT-GA) AND CORRELATION SCALOGRAM (CWT-CS) ANALYSES

Water table position	Variables	Marginal R^2	Conditional R^2	AIC	BIC
3 cm below peat surface n =76	WI	0.66	0.79	494.00	503.30
	$fBWI_{980}$	0.68	0.79	500.50	501.63
	CWT-GA	0.85	0.90	389.86	408.51
	CW-CS	0.76	0.82	454.05	468.04
7 cm below peat surface n =76	WI	0.39	0.62	-91.37	-82.55
	$fBWI_{980}$	0.41	0.59	-102.54	-85.90
	CWT-GA	0.75	0.75	-161.0	-143.44
	CW-CS	0.60	0.61	-151.72	-136.30

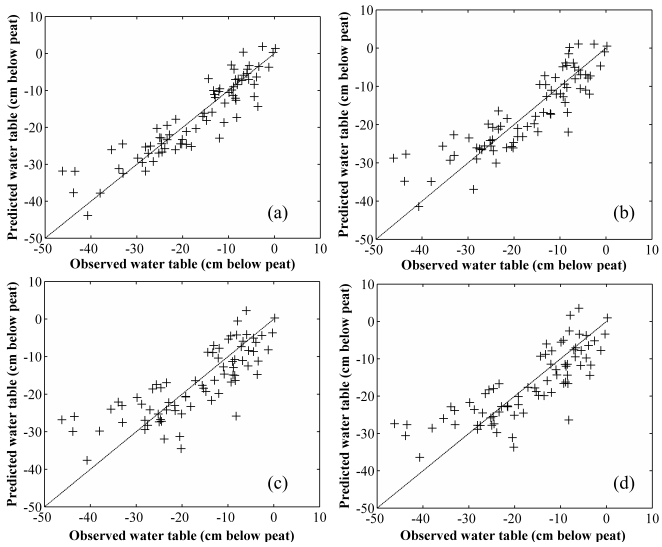

Fig. 3. Predicted versus observed plots related to WT height (cm below peat surface) at the PEATcosm site using spectral indices and wavelet features. Independent variables are (a) wavelet feature selected from the GA, (b) wavelet features selected from the correlation scalogram, (c) WI, and (d) fBWI980.

mation Criterion values compared with counterpart models with a reduced number of coefficients (results not shown here), suggesting the absence of overfitting in the more complex models. The differences between the marginal and conditional R^2 values for models based upon wavelet coefficients were lower (0.05 and 0.06 for CWT-GA and CWT-CS, respectively) than models based upon spectral indices (0.13 and 0.11 for WI and fBWI980, respectively). As is evident in Fig. 3, the relationship between predictions and observations for wavelet-based models was much stronger and characterized by minimum bias compared to models based upon spectral indices, which also showed significant overprediciton at lower WT values. The results for 7 cm VMC models were similar to that of WT, but a greater improvement in marginal R^2 was obtained with CWT-GA (Marginal $R^2 = 0.75$) compared with the spectral index models (marginal $R^2 = 0.39$ and 0.41 for WI and fBWI980, respectively).

IV. DISCUSSION

Previous studies have demonstrated the relationship between NIR spectral indices and surface moisture dynamics of vegetation in peatland ecosystems. Most recently, Meingast *et al.* [12] demonstrated the strength and consistency of these spectral indices across an extreme range of WT positions as well as with mixed species compositions. To our knowledge, previous studies have relied solely on spectral indices for estimating the moisture dynamics in peatland ecosystems, rather than exploring multivariate analysis combining information from multiple bands. In this paper, we demonstrated the utility of spectroscopy data for monitoring peatland moisture dynamics; the predictions of moisture content were significantly enhanced by incorporating CWT analysis. The analysis was carried out using the test data set, which contains significant variation in moisture ranges and vegetation diversity. This is broadly representative of northern peatland ecosystems.

The results of this paper showed that CWT coefficients explain more variation in surface moisture content and WT in peatlands compared with spectral indices. At the PEATcosm site, the conditional R^2 values from a linear mixed-effect model increased from 0.66 to 0.89 for WT and from 0.39 to 0.75 for 7 cm VMC using CWT coefficients selected by GA (CWT-GA) over the WI. Similar results were obtained for 7 cm VMC model at the Nestoria site with models based on CWT-GA (CV-R^2 = 0.66 and CV-RMSE = 0.08) outperforming those based on fWBI 980 (CV-R^2 = 0.51 and CV-RMSE = 0.13) and WI (CV-R^2 = 0.50 and CV-RMSE = 0.13). As evidenced in Fig. 2, a number of VMC values were clustered around 0.6 likely due to the insensitivity of the Thetaprobe instrument to larger VMC values. We performed further analysis by removing VMC observations exceeding 0.55 and found that the relationship between CWT-GA and VMC −7 cm remained essentially unchanged. However, the linear relationship further weakened for vegetation indices and CWT-CS when these values were removed. In comparison to VMC 7 cm, only a marginal improvement was obtained for VMC measured at 3 cm depth at the Nestoria site with wavelet-based models, providing statistical relationships with strengths slightly superior to those based on spectral indices. The superiority of CWT coefficients over spectral indices found in this paper is consistent with that from recent studies leveraging CWT for leaf and canopy level moisture prediction in forested ecosystems [18], [31]–[33], [52].

The superior performance of CWT coefficients in this analysis is likely the result of several factors. First, CWT analysis facilitates a multiple regression model development approach for estimating peatland moisture content. In addition to selecting multiple coefficients related to water absorption, the stepwise regression approach also allows the inclusion of other important wavelet coefficients that, although insensitive to variation in moisture content, are sensitive to other vegetation characteristics important for moisture dynamics and sensing. Among the five CWT-GA coefficients in the highest ranked WT model, three coefficients were related to water absorption regions (1148, 1242, and 1549 nm), one with a lignin absorption region (1735 nm; [48]), and one in the NIR region insensitive to leaf and canopy moisture, but related to leaf or vegetation structure (720 nm). Similarly, among the five CWT-GA coefficients in the best performing VMC

model at the PEATcosm site, one feature was related to a water absorption region (959 nm), one to a cellulose and protein absorption feature (2364 nm), two to the NIR region (711 and 741 nm), and one to visible wavelengths (535 nm) that are minimally influenced by vegetation moisture. The nonwater absorption-related wavelet coefficients included in the model potentially suppress the impact of extraneous factors that negatively contribute to *Sphagnum* reflectance such as vegetation structure and leaf dry matter, among others. Alternatively, water stress, in low WT conditions might cause physiological changes related to pigmentation and dry matter content in the *Sphagnum* canopy in addition to changes in the vegetation moisture content. CWT coefficients that are sensitive to changes in lignin or protein content and discoloration might have additionally captured this physiological variation, ultimately improving model accuracy. Finally, the fact that CWT coefficients were selected across various scales of wavelet decomposition also indicated a contributing factor for improved performance compared with other methods. The multiscale coefficients transform and represent the original reflectance spectrum in myriad forms: fine scale coefficients (Scales 1 and 2) capture abrupt changes in the amplitude of reflectance in narrow wavelength regions related to absorption features, while the medium scale coefficients (Scales 3–5) can account for changes in the depth and shape of absorption features, and coarser scale coefficients (Scales 6–10) capture subtle trends occurring over broader spectral intervals (e.g., NIR and SWIR) and the overall reflectance continuum [26], [28]. By including coefficients at different scales, the wavelet-based models account for multiscale dynamics related to the changing moisture condition of peatland vegetation, ultimately explaining greater variation in VMC and WT.

The spectral indices tested in this paper utilize a single water absorption region near 980 nm and a reference band near 920 nm. Such indices can greatly reduce the complexity of spectroscopy data by summarizing information into a single variable. While doing so, they also miss potentially rich and relevant information offered by highly dimensional data. Indeed, the performance of models based on the spectral indices was comparable to the wavelet-based models for VMC measured at 3 cm depth at Nestoria, but performed poorly for 7 cm VMC and WT. The weakening of the relationship from surface VMC to WT for spectral indices has been shown previously in [11]. These indices rely on changes in water held in thin surface tissues and therefore are only related to water content of the Sphagnum at the peatland surface due to the limited penetration of optical solar radiation into the canopy [49]. Our wavelet-based results indicate that the methods sensitive to changes in multiple leaf and canopy attributes are required to estimate WT position and VMC at greater depths as a function of spectral changes. Several studies in forested ecosystems have documented that the spectral indices relate poorly to leaf water content due to large spectral variability arising from the richness of species composition [18], [50], [51]. Similar results were observed in peatlands by Harris *et al.* [10] and Meingast *et al.* [12]. They reported that a variation in *Sphagnum* species, particularly S. rubellum, can significantly alter the relationship between spectral indices and WT position limiting their broader applicability in peatland ecosystems with diverse vegetation communities. Further problems related to atmospheric interference arise when data are collected from aircraft or satellite platforms. Sims and Gamon [50] showed that water vapor in the atmosphere results in several absorption bands that limit atmospheric transmittance. They found that the water absorption regions surrounding 980 nm used in the WI and fBWI980 indexes overlaps with a weak atmospheric water vapor absorption band, reducing their utility under high atmospheric water vapor conditions. In contrast, the other water absorption regions (1150–1260 and 1520–1540 nm) utilized by the wavelet-based models overlapped with regions of high atmospheric transmittance, strengthening their performance compared with the spectral index models. However, we caution that in ecosystem-level moisture mapping efforts involving several different hyperspectral image scenes, rigorous atmospheric correction effort is necessary to have consistent radiometric values across scenes before building wavelet-based prediction models.

We compared two different feature selection methods to select optimal subsets of CWT coefficients for describing variation in moisture content and WT position in peatland ecosystems. The results demonstrate that CWT coefficients selected by the GA (CWT-GA) outperformed coefficients selected from the correlation scalogram approach (CWT-CS). The GA was imbedded in multiple regression models and was constrained to minimize multicollinearity while maximizing prediction accuracy. On the contrary, the search process for the correlation scalogram method was independent of the modeling process, and the coefficients were selected based on their individual correlation with VMC and WT. The superior performance by CWT-GA models suggests that a model selection procedure that considers the impact of a suite of dependent variables on model quality (rather than a single variable at a time as in CWT-CS) results in higher model accuracy. CWT-GA included coefficients related to vegetation moisture as well as to leaf or vegetation structure indicative of the subsurface moisture condition. Taken together, these results suggest superior performance of the CWT-CS over spectral indices, indicating that wavelet coefficients are a useful feature selection tool.

GA selected an entirely different subset of best CWT features for VMC-7 cm between the PEATcosm and Nestoria sites. The PEATcosm site represents a controlled, experimentally manipulated study of vegetation and WT treatments. The spectra collected at this site are likely more consistent compared with those collected in a natural peatland such as the Nestoria site. Indeed, several factors such as microtopography (lawn, hummock, and hollow) and vegetation structure certainly contribute an additional source of spectral variation at the Nestoria site. The different subsets of CWT-GA features highlight the major limitation of all empirical models; they are site specific and are not readily extendible to new areas with different environmental conditions. Such differences might also have been due to the result of redundant information in hyperspectral data and subsequent CWT features leading to various combinations of optimum features. While these findings cannot be generalizable to all boreal landscapes with-

out further calibration at broader scales, incorporating whole-ecosystems, we note here that the plant functional groups involved are broadly representative of open poor fen and bog systems across North America.

In this paper, we did not exclude noisy bands in the atmospheric absorption regions (370–390, 1340–1450, 1790–2030, 2480–2500 nm) prior to calculating wavelet coefficients (similar to [52]). One of the primary strengths of wavelet analysis is its inherent ability to suppress high frequency noise into a small number of low-scale features. The GA would presumably exclude such noisy features in the feature selection process. However, we recognize that removing such noisy bands in the atmospheric absorption regions is a good practice and is recommended in future studies.

V. Conclusion

Our objective was to test the utility of the CWT analysis for estimating surface moisture content and WT in peatland ecosystems. Two sets of wavelet coefficients selected by a GA and from a correlation scalogram approach were examined along with best spectral indices found useful in previous studies. We found that CWT coefficients perform the best for monitoring both WT position and surface moisture content. CWT affords multiscale analysis of absorption features and the spectral continuum that offers an opportunity to capture the relevant information that is manifested at different scales. The spectral indices were correlated similarly with surface moisture content measured at 3 cm depth but performed poorly for VMC measured at 7 cm depth and WT position. Multiscale wavelet coefficients detect and isolate variation in the reflectance continuum and capture the shape and depth of absorption features not detectable in the original reflectance domain over broad and narrow spectral regions. Our results provide new insights into the significance of various spectral regions apart from water absorption regions to detect vegetation changes caused by extreme WT ranges. CWT identified regions that reflect changes in the physiology of the vegetation to aid in the prediction of VMC and WT. This further fortifies the ability of CWT analysis in predicting VMC and WT over simple indices limited to water absorption regions of the spectrum. We also demonstrated that selection of useful subset of variables using GA can provide improved estimates of moisture variables than more commonly used feature selection techniques based on correlation scalogram.

Acknowledgment

The authors would like to thank P. C. Timber for allowing this research to be conducted on the Nestoria Field site.

References

[1] E. Gorham, "Northern peatlands: Role in the carbon cycle and probable responses to climatic warming," *Ecol. Appl.*, vol. 1, no. 2, pp. 182–195, 1991.

[2] Z. Yu, J. Loisel, D. P. Brosseau, D. W. Beilman, and S. J. Hunt, "Global peatland dynamics since the last glacial maximum," *Geophys. Res. Lett.*, vol. 37, no. 13, p. L13402, 2010.

[3] N. T. Roulet and M.-K. Woo, "Low arctic wetland hydrology," *Can. Water Resour. J.*, vol. 11, no. 1, pp. 69–75, 1986.

[4] D. W. Hilbert, N. Roulet, and T. Moore, "Modelling and analysis of peatlands as dynamical systems," *J. Ecol.*, vol. 88, no. 2, pp. 230–242, 2000.

[5] S. D. Bridgham, J. Pastor, B. Dewey, J. F. Weltzin, and K. Updegraff, "Rapid carbon response of peatlands to climate change," *Ecology*, vol. 89, no. 11, pp. 3041–3048, 2008.

[6] B. P. Walter, M. Heimann, and E. Matthews, "Modeling modern methane emissions from natural wetlands: 1. Model description and results," *J. Geophys. Res.-Atmos.*, vol. 106, no. D24, pp. 34189–34206, 2001.

[7] S. Frolking, N. T. Roulet, T. R. Moore, P. M. Lafleur, J. L. Bubier, and P. M. Crill, "Modeling seasonal to annual carbon balance of Mer Bleue Bog, Ontario, Canada," *Global Biogeochem. Cycles*, vol. 16, no. 3, pp. 4-1–4-21, 2002.

[8] P. D. Moore and D. J. Bellamy, *Peatlands*. New York, NY, USA: Springer, 1976.

[9] R. G. Bryant and A. J. Baird, "The spectral behaviour of *Sphagnum* canopies under varying hydrological conditions," *Geophys. Res. Lett.*, vol. 30, no. 3, p. 1134, 2003.

[10] A. Harris, R. G. Bryant, and A. J. Baird, "Detecting near-surface moisture stress in *Sphagnum* spp.," *Remote Sens. Environ.*, vol. 97, no. 3, pp. 371–381, 2005.

[11] A. Harris, R. G. Bryant, and A. J. Baird, "Mapping the effects of water stress on *Sphagnum*: Preliminary observations using airborne remote sensing," *Remote Sens. Environ.*, vol. 100, no. 3, pp. 363–378, 2006.

[12] K. M. Meingast *et al.*, "Spectral detection of near-surface moisture content and water-table position in northern peatland ecosystems," *Remote Sens. Environ.*, vol. 152, pp. 536–546, Sep. 2014.

[13] E. Chuvieco, D. Riaño, I. Aguado, and D. Cocero, "Estimation of fuel moisture content from multitemporal analysis of landsat thematic mapper reflectance data: Applications in fire danger assessment," *Int. J. Remote Sens.*, vol. 23, no. 11, pp. 2145–2162, 2002.

[14] A. De Santis, P. Vaughan, and E. Chuvieco, "Foliage moisture content estimation from one-dimensional and two-dimensional spectroradiometry for fire danger assessment," *J. Geophys. Res.-Biogeosci.*, vol. 111, no. G4, p. G04S03, 2006.

[15] X. Yanfang, Z. Wenji, Z. Demin, and G. Huili, "Sensitivity analysis of vegetation reflectance to biochemical and biophysical variables at leaf, canopy, and regional scales," *IEEE Trans. Geosci. Remote Sens.*, vol. 52, no. 7, pp. 4014–4024, Jul. 2014.

[16] J. Letendre, M. Poulin, and L. Rochefort, "Sensitivity of spectral indices to CO_2 fluxes for several plant communities in a *Sphagnum*-dominated peatland," *Can. J. Remote Sens.*, vol. 34, no. 2, pp. S414–S425, 2008.

[17] L. Li, S. L. Ustin, and D. Riano, "Retrieval of fresh leaf fuel moisture content using genetic algorithm partial least squares (GA-PLS) modeling," *IEEE Geosci. Remote Sens. Lett.*, vol. 4, no. 2, pp. 216–220, Apr. 2007.

[18] T. Cheng, B. Rivard, and A. Sánchez-Azofeifa, "Spectroscopic determination of leaf water content using continuous wavelet analysis," *Remote Sens. Environ.*, vol. 115, no. 2, pp. 659–670, 2011.

[19] L. M. Bruce, C. Morgan, and S. Larsen, "Automated detection of subpixel hyperspectral targets with continuous and discrete wavelet transforms," *IEEE Trans. Geosci. Remote Sens.*, vol. 39, no. 10, pp. 2217–2226, Oct. 2001.

[20] L. M. Bruce and J. Li, "Wavelets for computationally efficient hyperspectral derivative analysis," *IEEE Trans. Geosci. Remote Sens.*, vol. 39, no. 7, pp. 1540–1546, Jul. 2001.

[21] M. J. Falkowski, A. M. S. Smith, A. T. Hudak, P. E. Gessler, L. A. Vierling, and N. L. Crookston, "Automated estimation of individual conifer tree height and crown diameter via two-dimensional spatial wavelet analysis of lidar data," *Can. J. Remote Sens.*, vol. 32, no. 2, pp. 153–161, 2006.

[22] G. A. Blackburn, "Wavelet decomposition of hyperspectral data: A novel approach to quantifying pigment concentrations in vegetation," *Int. J. Remote Sens.*, vol. 28, no. 12, pp. 2831–2855, 2007.

[23] G. A. Blackburn and J. G. Ferwerda, "Retrieval of chlorophyll concentration from leaf reflectance spectra using wavelet analysis," *Remote Sens. Environ.*, vol. 112, no. 4, pp. 1614–1632, 2008.

[24] A. Banskota *et al.*, "Investigating the utility of wavelet transforms for inverting a 3-D radiative transfer model using hyperspectral data to retrieve forest LAI," *Remote Sens.*, vol. 5, no. 6, pp. 2639–2659, 2013.

[25] A. M. S. Smith *et al.*, "Production of vegetation spatial-structure maps by per-object analysis of juniper encroachment in multitemporal aerial photographs," *Can. J. Remote Sens.*, vol. 34, no. 2, pp. S268–S285, 2008.

[26] A. Banskota, R. H. Wynne, and N. Kayastha, "Improving within-genus tree species discrimination using the discrete wavelet transform applied to airborne hyperspectral data," *Int. J. Remote Sens.*, vol. 32, no. 13, pp. 3551–3563, 2011.

[27] N. Ghasemi, M. R. Sahebi, and A. Mohammadzadeh, "Biomass estimation of a temperate deciduous forest using wavelet analysis," *IEEE Trans. Geosci. Remote Sens.*, vol. 51, no. 2, pp. 765–776, Feb. 2013.

[28] A. Banskota, R. H. Wynne, S. P. Serbin, N. Kayastha, V. A. Thomas, and P. A. Townsend, "Utility of the wavelet transform for LAI estimation using hyperspectral data," *Photogram. Eng. Remote Sens.*, vol. 79, no. 7, pp. 653–662, 2013.

[29] T. Cheng, B. Rivard, A. G. Sánchez-Azofeifa, J.-B. Féret, S. Jacquemoud, and S. L. Ustin, "Deriving leaf mass per area (LMA) from foliar reflectance across a variety of plant species using continuous wavelet analysis," *ISPRS J. Photogram. Remote Sens.*, vol. 87, pp. 28–38, Jan. 2014.

[30] A. Banskota *et al.*, "An LUT-based inversion of DART model to estimate forest LAI from hyperspectral data," *IEEE J. Sel. Topics Appl. Earth Observ. Remote Sens.*, vol. 8, no. 6, pp. 3147–3160, Jun. 2015.

[31] S. Ullah, A. K. Skidmore, M. Naeem, and M. Schlerf, "An accurate retrieval of leaf water content from mid to thermal infrared spectra using continuous wavelet analysis," *Sci. Total Environ.*, vol. 437, pp. 145–152, Oct. 2012.

[32] T. Cheng, B. Rivard, A. G. Sánchez-Azofeifa, J.-B. Féret, S. Jacquemoud, and S. L. Ustin, "Predicting leaf gravimetric water content from foliar reflectance across a range of plant species using continuous wavelet analysis," *J. Plant Physiol.*, vol. 169, no. 12, pp. 1134–1142, 2012.

[33] M. Kalacska, M. Lalonde, and T. R. Moore, "Estimation of foliar chlorophyll and nitrogen content in an ombrotrophic bog from hyperspectral data: Scaling from leaf to image," *Remote Sens. Environ.*, vol. 169, pp. 270–279, Nov. 2015.

[34] P. S. Addison, *The Illustrated Wavelet Transform Handbook*. London, U.K.: Institute of Physics Publishing, 2002.

[35] L. Kooistra, J. Wanders, G. F. Epema, R. S. E. W. Leuven, R. Wehrens, and L. M. C. Buydens, "The potential of field spectroscopy for the assessment of sediment properties in river floodplains," *Anal. Chim. Acta*, vol. 484, no. 2, pp. 189–200, 2003.

[36] J. C. Luo, J. Zheng, Y. Leung, and C. H. Zhou, "A knowledge-integrated stepwise optimization model for feature mining in remotely sensed images," *Int. J. Remote Sens.*, vol. 24, no. 23, pp. 4661–4680, 2003.

[37] C. Vaiphasa, A. K. Skidmore, W. F. de Boer, and T. Vaiphasa, "A hyperspectral band selector for plant species discrimination," *ISPRS J. Photogram. Remote Sens.*, vol. 62, no. 3, pp. 225–235, 2007.

[38] R. Behroozmand and F. Almasganj, "Optimal selection of wavelet-packet-based features using genetic algorithm in pathological assessment of patients' speech signal with unilateral vocal fold paralysis," *Comput. Biol. Med.*, vol. 37, no. 4, pp. 474–485, 2007.

[39] B. S. Aghazadeh, S. Ansari, R. Pidaparti, and K. Najarian, "Non-invasive estimation of intracranial pressure in traumatic brain injury (TBI) using fully-anisotropic Morlet wavelet transform and support vector regression," *Biomed. Eng. Lett.*, vol. 3, no. 3, pp. 190–197, 2013.

[40] L. Potvin, E. S. Kane, R. Chimner, R. K. Kolka, and E. A. Lilleskov, "Effects of water table position and plant functional group on plant community, aboveground production, and peat properties in a peatland mesocosm experiment (PEATcosm)," *Plant Soil*, vol. 387, no. 1, pp. 277–294, 2015.

[41] J. H. Holland, *Adaptation in Natural and Artificial Systems*. Ann Arbor, MI, USA: Univ. Michigan Press, 1975.

[42] Y.-C. Lin and K. Sarabandi, "Retrieval of forest parameters using a fractal-based coherent scattering model and a genetic algorithm," *IEEE Trans. Geosci. Remote Sens.*, vol. 37, no. 3, pp. 1415–1424, May 1999.

[43] J. Peñuelas, I. Filella, C. Biel, L. Serrano, and R. Savé, "The reflectance at the 950–970 nm region as an indicator of plant water status," *Int. J. Remote Sens.*, vol. 14, no. 10, pp. 1887–1905, 1993.

[44] J, B. D. Pinheiro, S. DebRoy, D. Sarkar, and R Core Team, NLME: Linear and nonlinear mixed effects models. R package version 3.1-118, 2014. [Online]. Available: https://cran.r-project.org/web/packages/nlme/

[45] S. Nakagawa and H. Schielzeth, "A general and simple method for obtaining R^2 from generalized linear mixed-effects models," *Methods Ecol. Evol.*, vol. 4, no. 2, pp. 133–142, 2013.

[46] J. S. Lefcheck. (Mar. 2013). *R2 for Linear Mixed Effects Models*. [Online]. Available: https://jslefche.wordpress.com/2013/03/13/r2-for-linear-mixed-effects-models

[47] H. W. Lilliefors, "On the Kolmogorov–Smirnov test for the exponential distribution with mean unknown," *J. Amer. Statist. Assoc.*, vol. 64, no. 325, pp. 387–389, 1969.

[48] R. F. Kokaly and R. N. Clark, "Spectroscopic determination of leaf biochemistry using band-depth analysis of absorption features and stepwise multiple linear regression," *Remote Sens. Environ.*, vol. 67, no. 3, pp. 267–287, 1999.

[49] D. A. Sims and J. A. Gamon, "Estimation of vegetation water content and photosynthetic tissue area from spectral reflectance: A comparison of indices based on liquid water and chlorophyll absorption features," *Remote Sens. Environ.*, vol. 84, no. 4, pp. 526–537, 2003.

[50] D. A. Sims and J. A. Gamon, "Relationships between leaf pigment content and spectral reflectance across a wide range of species, leaf structures and developmental stages," *Remote Sens. Environ.*, vol. 81, nos. 2–3, pp. 337–354, 2002.

[51] G. A. Sánchez-Azofeifa *et al.*, "Differences in leaf traits, leaf internal structure, and spectral reflectance between two communities of lianas and trees: Implications for remote sensing in tropical environments," *Remote Sens. Environ.*, vol. 113, no. 10, pp. 2076–2088, 2009.

[52] T. Cheng, D. Riaño, and S. L. Ustin, "Detecting diurnal and seasonal variation in canopy water content of nut tree orchards from airborne imaging spectroscopy data using continuous wavelet analysis," *Remote Sens. Environ.*, vol. 143, pp. 39–53, Mar. 2014.

Asim Banskota received the bachelor's degree in environmental science from Kathmandu University, Dhulikhel, Nepal, in 2002, the master's degree in geoinformation science and earth observation from ITC, Enschede, The Netherlands, in 2007, and the Ph.D. degree in geospatial and environmental analysis from the Virginia Polytechnic Institute and State University, Blacksburg, VA, USA, in 2011.

He was with the Center for Rural Technology, Nepal and Resources Himalaya Foundation, Patan, Nepal, at different capacities before joining the Ph.D. program. He was a Senior Remote Sensing Analyst with Conservation International, Arlington, VA, USA, a Research Assistant Professor with Michigan Technological University, Houghton, MI, USA, and a Research Associate with the Department of Forest Resources, University of Minnesota, Minneapolis, MN, USA. He is currently a Geospatial Data Scientist with Monsanto, St. Louis, MO, USA. His current research interests include remote sensing applications to study vegetation condition and terrestrial ecosystem dynamics.

Michael J. Falkowski received the B.S. degree in geography and geology from the University of Wisconsin, Stevens Point, WI, USA, in 2000, and the M.S. degree in forestry and the Ph.D. degree in natural resources from the University of Idaho, Moscow, ID, USA, in 2005 and 2008, respectively.

He held faculty appointments with Michigan Technological University, Houghton, MI, USA, the University of Minnesota at St. Paul, St. Paul, MN, USA, and Colorado State University, Fort Collins, CO, USA, where he has been an Associate Professor of Remote Sensing with the Department of Ecosystem Science and Sustainability since 2015. His current research interests include the development and application of accurate and efficient methods to characterize, measure, and monitor vegetation structure, composition, and function across large spatial extents.

Alistair M. S. Smith received the B.Sc. degree in physics from the University of Edinburgh, Edinburgh, U.K., and the M.Sc. degree in imaging and digital image processing and the Ph.D. degree in geography from the University of London, London, U.K.

He is an Associate Professor of Environmental Biophysics with the University of Idaho, Moscow, ID, USA, where he is the Director of the Idaho Fire Institute for Research and Education and the Director of Research and Graduate Studies with the College of Natural Resources.

Evan S. Kane received the B.S. degree in applied ecology and the M.S. degree in forestry from Michigan Technological University, Houghton, MI, USA, in 1999 and 2001, respectively, and the Ph.D. degree in forest ecology from the University of Alaska, Fairbanks, AK, USA, in 2006.

He was an Assistant Professor with the School of Forestry, Michigan Technological University, and a Collaborative Research Scientist with the U.S. Forest Service Northern Research Station, Houghton. His research focusses on belowground processes, with an emphasis on carbon cycle dynamics in boreal and temperate forested and wetland ecosystems. His research addresses belowground processes following disturbances, such as harvesting, wildfires, or drought, and examines how these processes are likely to change with a changing climate.

Karl M. Meingast received the B.S. degree in applied physics and the M.S. degree in forest ecology and management from Michigan Technological University, Houghton, MI, USA, in 2011 and 2013, respectively. He is currently working toward the Ph.D. degree in forest science with his advisor Dr. Evan S. Kane at Michigan Technological University.

His research focusses on dissolved organic carbon dynamics across the terrestrial-river-coastal interface of Lake Superior. He is particularly interested in understanding the link between winter climate and flushing of organic matter during snowmelt. His research is funded by the NASA Earth and Space Sciences Fellowship Program.

Laura L. Bourgeau-Chavez received the B.S. degree in forest ecology and the M.S. degree in forest ecology and remote sensing from the University of Michigan, Ann Arbor, MI, USA, in 1987 and 1994, respectively, and the Ph.D. degree in forestry and remote sensing from the University of New Brunswick, Fredericton, NB, Canada, in 2014.

She was a Research Scientist with the Environmental Research Institute of Michigan (ERIM), Ann Arbor. She continued to conduct research at ERIM International, Ann Arbor, Veridian, Ann Arbor, and General Dynamics, Ann Arbor (all heritage ERIM) until 2007, and then moved to the Michigan Tech Research Institute (MTRI), Michigan Technological University, Houghton, MI, USA, where she is currently a Senior Research Scientist and an Adjunct Associate Professor. She was with the Environmental Science Laboratory at MTRI. Her current research interests include the development of remote sensing technology to map and monitor landscape ecosystems, including vegetation structure, hydrological state, dominant covertype, and developing applications of synthetic aperture radar.

Mary Ellen Miller received the B.A. degree in physics from SUNY Geneseo, Geneseo, NY, USA, the M.S. degree in imaging science from the Rochester Institute of Technology, Rochester, NY, USA, and the Ph.D. degree in environmental engineering from the University at Buffalo, Buffalo, NY, USA.

She is currently a Research Engineer with the Michigan Tech Research Institute, Michigan Technological University, Ann Arbor, MI, USA. She has over 15 years of experience solving problems in the fields of GIS, Environmental Remote Sensing, and Environmental Modeling. Her current research interests include developing practical methods of supporting land management with remote sensing and environmental modeling, large-scale mapping of vegetation, land cover and land use change, developing and improving environmental models, and improving modeling tools for postfire risk assessment and remediation.

Nancy H. French has been involved in applications of remote sensing to ecology and vegetation studies for more than 25 years. Her current research interests include the study of forest ecosystems and the application of remote sensing techniques to ecosystem studies, developing approaches to use satellite data to monitor the spatial and temporal patterns of wildland fire and its impact on terrestrial ecosystems and the carbon cycle. She is a Co-Principal Investigator for the Fire and Smoke Model Evaluation Experiment, which aims to improve operational smoke modeling through a multidisciplinary science-based experiment at large prescribed burns across the U.S., and the Principal Investigator for MichiganView, which is a part of AmericaView, a nationwide partnership of remote sensing scientists who support the use of Landsat and other public-domain remotely sensed satellite data through applied remote sensing research, K-12, and higher STEM education, workforce development, and technology transfer.

View publication stats